Journal of Marine Science and Application (2024) 23: 927-946
https://doi.org/10.1007/s11804-024-00540-0

RESEARCH ARTICLE

Optimal Path Following Controller Design Based on Linear Quadratic Regulator for Underactuated Ships in Varying Wave and Wind Conditions

Abbas Ghassemzadeh[1], Haitong Xu[1] and C. Guedes Soares[1]

Received: 29 April 2024 / Accepted: 01 May 2024

Abstract

This study presents an optimisation-based approach for determining controller gains in ship path-following under varying sea states, wave, and wind directions. The dynamic Line of Sight approach is used to regulate the rudder angle and guide the Esso Osaka ship along the desired path. Gains are optimised using a genetic algorithm and a comprehensive cost function. The analysis covers a range of wave attack directions and sea states to evaluate the controller performance. Results demonstrate effective convergence to the desired path, although a steady-state error persists. Heading and rudder angle performance analyses show successful convergence and dynamic adjustments of the rudder angle to compensate for deviations. The findings underscore the influence of wave and wind conditions on ship performance and highlight the need for precise gain tuning. This research contributes insights into optimising and evaluating path-following controllers for ship navigation.

Keywords Ship manoeuvring; Optimal control; Wave and wind forces; Genetic algorithm; LQR control

1 Introduction

Navigating at sea without wind and waves is rare, and ships are often affected by these environmental disturbances, causing them to deviate from their course (Kim et al. 2022; Kim and Tezdogan, 2022; Ma et al. 2022; Seo et al. 2019; Skejic and Faltinsen, 2013; Zhang et al. 2019; Xu et al. 2024). As a result, characterising these disturbances is crucial for designing effective motion controllers and understanding the limitations that may prevent the design from meeting performance specifications (Das and Talole, 2015; Yang et al., 2020).

Tracking records in autonomous surface ships reveal that various control design strategies have been proposed for surface ships, focusing on calm water (Kim et al., 2019; Xu et al., 2021; Sayyaadi & Ghassemzadeh, 2018). Similarly, for wavy conditions, for instance, Jiang and Xia (2022) proposed a sliding mode controller for a group of surface ships that accounts for environmental disturbances. However, most control methodologies have been devised specifically for ships at a scale representative of models, thereby accompanying inherent constraints such as parameter uncertainty, external perturbations, and other related factors.

For additional support, the idea that adverse weather conditions can affect the performance of the ship controller, referring to research studies by Yang et al. (2020), McTaggart (1992), and Li et al. (2021) is clarified. A robust nonlinear model predictive control (NMPC) approach (Yang et al., 2020) is introduced for dynamic positioning (DP) ships, addressing challenges posed by time-varying environmental disturbances and input saturation. The key objective is to guide perturbed DP vessels along predefined reference trajectories. To tackle this, the authors design a non-linear disturbance observer (NDO) to estimate unknown distur-

Article Highlights

- The study introduces a novel approach to optimising controller gains, considering diverse sea states, waves, and wind directions. This dynamic approach ensures effective path following even in challenging maritime conditions.
- Compared to classical PID controllers, the proposed controller exhibits robust performance, with smoother outputs and lower actuator deviations. Its efficiency in maritime control applications surpasses traditional methods, highlighting its potential for real-world implementation.
- Through comprehensive analysis, the study elucidates how waves and wind impact controller performance, particularly in sea states above 3. Variations in controller gains across different environmental conditions underscore the importance of accounting for these factors in control strategy design.
- Despite steady-state errors, the controller effectively guides the ship towards the desired path.

✉ Abbas Ghassemzadeh
abbasali@centec.tecnico.ulisboa.pt

[1] Centre for Marine Technology and Ocean Engineering (CENTEC), Instituto Superior Técnico, Universidade de Lisboa, Lisboa, Portugal

bances, incorporating these estimates into the NMPC optimisation model to effectively reject disturbances. Notably, the study achieves partial asymptotic stability in NMPC without the need for terminal costs or constraints, with simulations validating the proposed NDO-based NMPC's effectiveness and robustness in both setpoint regulation and trajectory tracking modes. McTaggart (1992) investigated the use of an adaptive controller to control the surge motion of a ship under wave action and showed that the adaptive controller effectively reduced surge motion and improved the ship's control system performance. Li et al. (2021) presented a model predictive control approach for path planning and tracking a ship under varying wind and wave conditions, effectively compensating for environmental disturbances and improving the ship's path planning accuracy.

The mentioned research studies reasonably clarify that the effects of environmental disturbances from wind and waves are significant and worth considering in controller design.

On the other hand, delving into more details about the model used in the previously researched study, considering both calm water situations and situations presenting environmental effects from waves and winds, reveals that recent research in ship control design highlights the limited attention given to full-scale autonomous ships. It is undeniable that the recent trend is using autonomous ships in transportation all over the world and due to the unpredictable nature of sea conditions and routes, full-scale ships are required for investigation in the area of effective control. Similarly, along with calm sea conditions, wave and wind sea conditions should also be considered on a full scale because it is still questionable whether the calm water situation can address all the challenges in designing controllers for autonomous ships.

Even though extensive experimental studies are conducted on scale models to monitor the performance of design controllers in environments close to reality, it should be noted that the scale factor plays a critical role in ensuring the accuracy of results. On the other hand, the models used in these tests are usually scale models, with the length of the model limited to 10 meters or less (Jafari et al., 2018). For instance, in (Woo et al., 2019; Ghassemzadeh et al., 2023), it could be seen that the considered ships have an overall length smaller than 10 meters.

In evaluating controllers designed for autonomous ships, the path-following controller is one of the most attractive areas that captivate many researchers. Path following is crucial for ship collision avoidance and safe navigation due to traffic issues and depth limitations in coastal areas.

Massive research has been done in the field of path-following control. Moreira et al. (2007) developed state feedback linearisation, and a dynamic Line of Sight vector norm was proposed for path-following control using the model ship characteristics of the Esso Osaka ship. Hinostroza et al. (2018), Xu et al. (2020), and Xu and Guedes Soares (2016a, b) used the vector field strategy for the path-following controller without considering environmental forces and moments. More recently, research studies by Chen et al. (2023), Codesseira and Tannuri (2021), and Zhang et al. (2022) deserve mention. These papers contribute to the advancement of path-following control strategies, hence, focusing on this objective in designing controllers for natural environments to evaluate the effects of waves and wind is worthwhile.

Conducting full-scale ship studies has also contributed to various subjects, such as path generation (Du et al., 2021; Xu et al., 2019), the effect of waves on circular motion (Li and Zhang, 2022), improving the course-keeping system (Min and Zhang, 2021) and estimating hydrodynamic coefficients (Kim, 2018). Similarly to the mentioned research studies, Mei et al. (2020) introduced a pioneering method for enhancing the accuracy of full-scale ship manoeuvring models, effectively addressing challenges arising from wind, waves, and sea currents. They meticulously corrected full-scale sea trial data by calculating wind and wave drift forces, fine-tuning parameters, and identifying essential hydrodynamic coefficients. This rigorous approach significantly improved the precision of full-scale data and bolstered the reliability of ship design and safety assessments. Furthermore, Yu et al. (2021) conducted a comprehensive evaluation of full-scale container ships using body-force models, particularly emphasising understanding the scale effect in simulations.

Despite the importance of full-scale ship effects and scale parameters on the performance of ship manoeuvrability, extensive research studies have also highlighted varying sea conditions, revealing that assuming calm water may not apply everywhere. As Bitner-Gregersen et al. (2016) have asserted, the met-ocean environment is influenced by geographic region and location-specific factors. Adverse weather conditions cannot encompass all the idiosyncrasies of the local met-ocean climate.

Extensive research studies have been conducted to model the variability and uncertainty of sea states concerning climate. Bitner-Gregersen et al. (2022) emphasise the importance of incorporating geographical variations in wave climate when designing ships, particularly considering the intended operating regions. Ship designs should be tailored to the prevailing wave characteristics and conditions specific to those areas. However, advancements in data collection techniques have enabled the acquisition of long-time series of sea surface elevation from wave rider buoys or offshore platforms. These measurements have facilitated the characterisation of sea states using directional sea wave spectra. By incorporating the information provided by directional wave spectra, a more comprehensive understanding of the climatic variability of sea states can be achieved, surpassing the limitations of solely relying on significant

wave height or the joint distribution of *Hs* and peak period.

Analysing the direction and wave height distribution presented in (Bitner-Gregersen et al., 2022), it is evident that in the most common shipping routes (Vettor and Guedes Soares, 2015), significant wave heights range from 0 to 8 meters. Similarly, the data analysed by (Lucas et al., 2011) also indicates that significant wave heights predominantly fall within the range of 1 to 6 meters for specific areas, and as shown in (Neary and Ahn, 2023), the largest significant wave height in Southern India Ocean is found at 5.0 m. Furthermore, an experiment in a specific area of China conducted by Cai et al. (2023) demonstrates that the most accurately predicted sea state in that region is up to sea state 5. Therefore, it is important to note that accurate predictions of variability and uncertainty in sea states should consider specific geographical areas and data availability over a certain period (Bitner-Gregersen et al., 2022; Lucas et al., 2011).

Prior research has shown that limited attention has been given to the study of full-scale autonomous ships. Results revealed that scale effects play a crucial role in the performance of the ship. Therefore, significant concern should be directed toward this aspect when designing controllers for real-world situations.

Following the relevant research, the present research aims to develop a control strategy for path-following purposes of a large tanker ship in the presence of sea waves and wind, utilising the Linear Quadratic Regulator (LQR) method. The full-scaled manoeuvring model of the Esso Osaka tanker is used to design a controller for path-following purposes. The main reason for selecting this model is its highly complex dynamics, making it more applicable to general cases compared to simplified or linear models.

The LQR control strategy is utilised to calculate the desired rudder angle, while a first-order Nomoto model for heading dynamics is considered to simplify the design procedure. LQR has been found to be applicable in autonomous ship control for heading angle regulation during path-following operations. For instance, Zhang et al. (2021) employed LQR in conjunction with non-linear control strategies to design an autonomous ship capable of accurately adhering to desired trajectories. Furthermore, the effectiveness of this approach has been rigorously assessed in studies such as Chen et al. (2023), and Tiwari and Krishnankutty (2021), revealing its favourable compatibility within the Multi-Input Multi-Output (MIMO) control domain. This approach presents a novel avenue for addressing the intricate challenges associated with ship manoeuvring, including tasks such as ship docking.

The other main assumption in this research involves the utilisation of the first-order Nomoto Model for rudder dynamics. This model has been extensively utilised in studies focusing on ship control systems (Sutulo and Guedes Soares, 2024). Several scientific papers have documented its widespread application and highlighted its contribution to understanding ship manoeuvring dynamics. For instance, Ren et al. (2018) introduced the adaptive Nomoto model to deal with the path-following problem of ships. Terada and Matsuda (2023) conducted a comprehensive study highlighting the effectiveness of the non-linear first-order model in accurately expressing the manoeuvring motion of ships with a minimal set of parameters. Their findings provide valuable scientific insights into the practical application of this model for ship control systems. In addition to the mentioned research studies, a variety of other research papers have also recognised and employed this model as well, such as Aung and Umeda (2020), Banazadeh and Ghorbani (2013), Feng et al. (2014), Lan et al. (2023), and Zhu et al. (2020). Utilising the Nomoto model involves identifying its parameters. These two parameters, T and K, are computed using the analytical method proposed by Journée (2001).

As previously clarified, there is still no clear perspective on utilising full-scale ship performance, especially in controller design in the presence of waves and wind. Therefore, to continue incorporating full-scale ship data into controller design, this research contributes in the following aspects.

Due to the variety of sea conditions resulting from different waves, wind forces, and directions, this research aims to develop an optimal controller uniquely suited to address the complexities posed by a wide range of sea states. Additionally, by comparing the results for moderate seas and calm water situations, this study compares the differences between considering wave environments and calm water, drawing conclusions on the assumption of including waves and wind in the design procedure. The aim is to create an effective controller that excels in the face of ever-changing sea conditions, enabling ships to manoeuvre efficiently, safely, and with precision, regardless of the challenges posed by the varying sea states. While there are several classifications of sea states, the analysis is limited to five sea states, namely, sea states 1 to 5. Consequently, it is essential to incorporate sea states 4 and 5 into the current analysis to assess the controller performance in intense wave conditions, as recommended by the International Maritime Organization (2021). Considering sea states 1 to 5 can provide a comprehensive description of the prevailing conditions.

Second, to assess the performance of the controller, four cost functions, namely, the maximum deviation from the initial position, reaching time to the desired path, maximum overshot in heading angle from the desired heading, and path following steady-state error, are considered.

After that, a genetic algorithm is employed to obtain the controller gain in each situation. Overall, this study contributes to the development of more efficient and effective path-following control strategies for vessels in the pres-

ence of wave and wind disturbances.

Lastly, to assess the robustness of the proposed controller in the presence of model disturbances, a white noise signal is introduced to the controller input as model disturbances and the performance of the proposed controller in this scenario is evaluated. Similarly, all the results are compared with a PID controller to compare the proposed controller and PID. The objective of this step is to provide more acceptable logic regarding the superiority of the proposed controller.

It should be noted that, in recent years, researchers have explored innovative approaches to enhance path-following control for under-actuated vessels. These advancements leverage machine learning techniques, such as deep reinforcement learning (Qu et al., 2023) focused on under-actuated unmanned surface vessels experiencing unmodeled dynamics and external disturbances, and neural networks (Ren et al., 2023; Bali et al., 2024; Deng et al., 2020) explored a model predictive control approach that explicitly accounts for uncertainties in vessel dynamics and environmental disturbances. However, the mentioned technique is still challenging. For instance, machine learning-based controllers lack the same level of theoretical stability guarantees as classical control methods like LQR and PID (Astolfi et al., 2007). Additionally, they involve numerous hyperparameters that require tuning. Finding optimal hyperparameters can be time-consuming and computationally expensive (LeCun et al., 2015). In the same way, machine learning models are often considered black boxes. Understanding how they arrive at control decisions can be challenging (Ribeiro et al., 2016). Machine learning controllers rely heavily on data and may struggle to generalise to unseen scenarios. Collecting sufficient high-quality data for training and validation can be difficult, especially in marine environments (Schmidhuber, 2015; Boyd and Vandenberghe, 2004). Also, deploying machine learning models in real-time control systems can be complex. High computational demands and latency issues may also arise (Sutton and Barto, 2018).

The remainder of the paper is structured as follows. Section 2 presents the dynamic manoeuvring model of the Esso Osaka ship. Section 3 calculates the forces and moments associated with the waves and wind, followed by an illustration of their effects on the ship's manoeuvring through the simulation of circular motion. Section 4 presents the LQR control strategy, the dynamic Line of Sight method for calculating the desired angle, and the first-order Nomoto model and its parameter calculation. Section 5 details the procedure for defining the optimal controller gain based on the Genetic Algorithm and associated cost function. The results and discussion are presented in Section 6 to evaluate the proposed controller performance and the results obtained. Finally, the conclusions are given in Section 7.

2 Non-linear manoeuvring model

It is convenient to use 6 Degrees of Freedom (DOF) to describe the motion of rigid bodies. These 6 DOF include three linear motions (surge, sway, and heave) along axes and three rotational motions (pitch, roll, and yaw), as shown in Figure 1. This model is necessary for simulation because through this model the inputs/outputs relations are described.

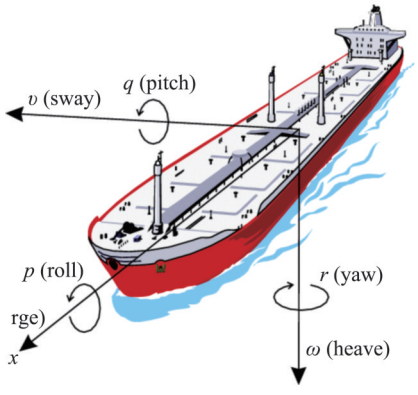

Figure 1 State variables in 6 DOF for the ship motions

In the context of still-water surface ship manoeuvring, neglecting the pitch and heave modes is common practice. Consequently, the equations governing heave and pitch are omitted, and it is assumed that their respective variables and derivatives are all zero (i.e., $w=q=\dot{w}=\dot{q}=0$). Similarly, if the motion is described in manoeuvring axes, it is also assumed that the roll rate and its derivative are zero everywhere except in the roll equation (Sutulo and Guedes Soares, 2011).

These simplifications are often made to ease the analysis and reduce computational complexity. However, it is important to note that by neglecting these modes and certain cross-coupling terms, the resulting three degrees of freedom (3DOF) equations in manoeuvring axes may not be entirely accurate. This is because the moments of inertia and the vertical coordinate of the centre of mass may not remain constant, although this effect is typically disregarded when the roll angles are moderate (Sutulo and Guedes Soares, 2011).

By adopting this scientific approach, the simplifications and assumptions made in still-water surface ship manoeuvring can be better understood. While these simplifications may lead to some inaccuracies, they serve as practical approximations and enable efficient analysis and simulation. As described in (Fossen, 2011; Sutulo and Guedes Soares, 2011), this coordinate system is sufficient to achieve a suitable and accurate model for marine surface ships.

The mathematical model implied in this study is obtained from (Abkowitz, 1980). In general, the equation of motion

is presented based on the centre of gravity. However, measuring forces are carried out based on the mid-ship position because the ship's centre of gravity is changed due to loading conditions. Hence, motion's equation is often described based on the centre of gravity, using hydrodynamic forces measured at the mid-ship position. Longitudinal force and lateral force are not affected by measuring position. However, the measured yaw moment is changed by the location of the measuring sensor (ITTC, 2000). This description is the background for the basic principles of ship hydrodynamic equations based on hydrodynamic parameters. These hydrodynamic parameters are determined using different system identification methods. In these methods, parameters are identified by measuring the forces in different directions as well as the moments applied to the ship. More details on how these methods are applied to calculate the hydrodynamic parameters can be found in (Xu et al., 2020; 2019).

The full-scale manoeuvring model of the Esso Osaka tanker, as shown in Figure 2 and Table 1, is used to design a controller for path-following purposes.

Figure 2 Esso Osaka tanker

Table 1 Major data of the Esso Osaka tanker (Li, 2004)

Length overall (m)	343
Length between perpendiculars (m)	325
Breadth moulded (m)	53
Depth moulded (m)	28.30
Assigned Summer Freeboard draft, extreme (m)	22.9
Design load draft moulded (m)	22.05
Full load displacement at assigned summer freeboard draft (mt)	328 880
Block coefficient, summer freeboard draft	0.831
Number of Rudder	1
Rudder area (m^2)	119.817
Longitudinal CG at trials; Forward of amidship (m)	10.30
Propeller Diameter (m)	9.1
Propeller Expanded area (m^2)	44.33
Propeller project area (m^2)	37.22
Propeller disk area (m^2)	65
Propeller rotation (r/min)	81

The main reason for selecting this model is its highly complex dynamics, making it more applicable to general cases than simplified or linear models. The complete 3DOF mathematical model of the Esso Osaka tanker is described by (Moreira et al., 2007):

$$\dot{u} = \frac{f_1 + \chi_e}{m - X_{\dot{u}}} \tag{1}$$

$$\dot{v} = \frac{1}{f_4}\left[\left(I_z - N_{\dot{r}}\right)\left(f_2 + Y_e\right) - \left(mx_G - Y_{\dot{r}}\right)\left(f_3 + H_e\right)\right] \tag{2}$$

$$\dot{r} = \frac{1}{f_4}\left[\left(m - Y_{\dot{v}}\right)\left(f_3 + H_e\right) - \left(mx_G - N_{\dot{v}}\right)\left(f_2 + Y_e\right)\right] \tag{3}$$

where:

$$\begin{aligned} f_1 = {} & \eta_1'\left[\frac{\rho}{2}L^2\right]u^2 + \eta_2'\left[\frac{\rho}{2}L^3\right]nu + \eta_3'\left[\frac{\rho}{2}L^4\right]n^2 \\ & - C_R'\left[\frac{\rho}{2}Su^2\right] + X_v'^2\left[\frac{\rho}{2}L^2\right]v^2 + +X_{e^2}'\left[\frac{\rho}{2}L^2c^2\right]e^2 \\ & +\left(X_{r^2}' + m'x_G'\right)\left[\frac{\rho}{2}L^4\right]r^2 + \left(X_{vr}' + m'\right)\left[\frac{\rho}{2}L^3\right]vr \\ & +X_{v^2r^2}'\left[\frac{\rho}{2}L^4U^{-2}\right]u^2r^2 \end{aligned} \tag{4}$$

$$\begin{aligned} f_2 = {} & Y_O'\left[\frac{\rho}{2}L^2\left(\frac{u_{A\infty}}{2}\right)^2\right] + \left\{Y_v'\left[\frac{\rho}{2}L^2U\right]v \right. \\ & \left. +Y_\delta'\left(c - c_0\right)\left[\frac{\rho}{2}L^2v\right]\right\} + \left\{\left(Y_r' - m'u'\right)\left[\frac{\rho}{2}L^3U\right]r \right. \\ & \left. - \frac{Y_\delta'}{2}\left(c - c_0\right)\left[\frac{\rho}{2}L^3r\right]\right\} + Y_\delta'\left[\frac{\rho}{2}L^2c^2\right]\delta \\ & +Y_{r^2v}'\left[\frac{\rho}{2}L^4U^{-1}\right]r^2v + Y_{e^3}'\left[\frac{\rho}{2}L^2c^2\right]e^3 \end{aligned} \tag{5}$$

$$\begin{aligned} f_3 = {} & N_O'\left[\frac{\rho}{2}L^3\left(\frac{u_{A\infty}}{2}\right)^2\right] + \left\{N_v'\left[\frac{\rho}{2}L^3U\right]v \right. \\ & \left. - N_\delta'\left(c - c_0\right)\left[\frac{\rho}{2}L^3v\right]\right\} + \left\{\left(N_r' - m'x_G'u'\right)\left[\frac{\rho}{2}L^4U\right]r \right. \\ & \left. +\frac{N_\delta'}{2}\left(c - c_0\right)\left[\frac{\rho}{2}L^4r\right]\right\} + N_\delta'\left[\frac{\rho}{2}L^3c^2\right]\delta \\ & +N_{r^2v}'\left[\frac{\rho}{2}L^5U^{-1}\right]r^2v + N_{e^3}'\left[\frac{\rho}{2}L^3c^2\right]e^3 \end{aligned} \tag{6}$$

$$\begin{aligned} f_4 = {} & \left(m' - Y_{\dot{v}}'\right)\left[\frac{\rho}{2}L^3\right]\left(I_z' - N_{\dot{r}}'\right)\left[\frac{\rho}{2}L^5\right] \\ & - \left(m'x_G' - N_{\dot{v}}'\right)\left[\frac{\rho}{2}L^4\right]\left(m'x_G' - Y_{\dot{r}}'\right)\left[\frac{\rho}{2}L^4\right] \end{aligned} \tag{7}$$

In Eq.1 to 7, u, v, and r are velocities in the surge, sway, and yaw direction, respectively. The velocity rate changes in 3 DOF are calculated through Eq. 1 to 7. m and x_G are the mass and longitudinal location of the Center of Gravity calculated from amidships. ρ is the water density, n is the propeller rotation speed (r/min), S is the wetted surface of the ship, and L is the overall length of the ship. The parameter f_1 captures the net effect of terms related to thrust forces (η_1', η_2', η_3'), added mass effects ($X_{\dot{e}^2}'$, $X_{\dot{r}^2}'$, $X_{\dot{v}r}'$, $X_{\dot{v}^2r^2}'$, $X_{\dot{v}}'^2$) resistance forces C_R' on the rate of change of 'u.' f_2 represents the combined influence of hydrodynamic coefficients for lateral forces (Y_O', $Y_{\dot{v}}'$, $Y_{\dot{\delta}}'$, $Y_{\dot{r}}'$, $Y_{\dot{r}^2\dot{v}}'$, $Y_{\dot{e}^3}'$) on the rate of change of 'v' as the ship moves laterally. f_3 represents the combined effect of the hydrodynamic coefficients for yaw moments (N_O', $N_{\dot{v}}'$, $N_{\dot{\delta}}'$, $N_{\dot{r}}'$, $N_{\dot{r}^2\dot{v}}'$, $N_{\dot{e}^3}'$) on the rate of change of 'r' as the ship rotates. f_4 represents the coupling between lateral and yaw motions, indicating how changes in one motion component can affect another

The forces and moment belonging to the wave and wind on the ship are presented as χ_e, wind and wave forces in surge direction, Υ_e, wave and wind force acting in the sway direction, and H_e, is the yaw moment exposed by the wave and wind in the yaw direction. These three components are described in the next section.

The U is the advance speed of the ship, and c is the effective longitudinal inflow velocity considering the presence of propeller calculated by:

$$U = \sqrt{u^2 + v^2} \tag{8}$$

$$c = \sqrt{\frac{A_P}{A_R}\left[(1-w)u + ku_{A\infty}\right]^2 + \frac{A_R - A_P}{A_R}(1-w)^2u^2} \tag{9}$$

The c_0 refers to the flow speed value in the equilibrium condition of the ship's forward velocity and propeller speed in straight-ahead motion. A_p, and A_R are the propeller and the rudder area, respectively. The wake fraction factor is w and $u_{A\infty}$ is the value given to the induced axial velocity calculated by (McTaggart, 2008):

$$u_{A\infty} = U(1-w)\sqrt{1 + C_{th}} \tag{10}$$

where C_{th} is the propeller thrust loading coefficient calculated by (McTaggart, 2008):

$$C_{th} = \frac{F_{\text{prop}}}{\frac{1}{2}\rho U^2(1-w)^2\frac{\pi}{4}D^2} \tag{11}$$

The effective rudder angle, e, in Eq.4 to Eq.7 is given by (Abkowitz, 1980):

$$e = \delta\frac{v}{c} + \frac{rL}{2c} \tag{12}$$

where δ is the rudder angle. All the nondimensional hydrodynamic coefficients are presented in Table 2.

3 Non-linear manoeuvring model

Environmental forces and moments caused by waves and wind are critical factors that must be considered when designing control strategies for ship path following. These forces vary according to the sea conditions and the hull shape and can result in the ship deviating from its intended course. Accurate modelling of these forces is crucial in developing a robust control strategy that ensures safe and efficient ship navigation.

One of the widely used methods for calculating environmental forces and moments is through mathematical relationships. These relationships are typically based on the principles of hydrodynamics and are derived from experimental or numerical data (Fossen, 2011).

Table 2 Hydrodynamic coefficients of the Esso Osaka tanker (Moreira et al., 2007)

Coefficient	Value	Coefficient	Value	Coefficient	Value
$\left(m - Y_{\dot{v}}\right)'$	0.035 2	$Y_{\dot{r}^2\dot{v}}'$	0.006 11	X_v'	0.030 70
$\left(I_z - N_{\dot{r}}\right)'$	0.002 22	$X_{\dot{e}^2}'$	−0.002 24	$mx_G - Y_{\dot{r}}$	0.000 572 0
Y_v'	−0.026 1	$X_{\dot{v}^2r^2}'$	−0.007 15	$(X_{vr}' + m')$	0.026 6
Y_r'	0.003 65	$N_{\dot{e}^3}'$	0.001 16	N_O'	−0.000 28
N_v'	−0.010 5	$N_{\dot{r}^2\dot{v}}'$	−0.045 0	$mx_G + X_{\dot{r}^2}$	0.005 720
N_r'	−0.004 80	η_1'	-0.962×10^{-5}	$mx_G - N_{\dot{v}}$	0.000 572 0
$Y_{\dot{\delta}}'$	−0.002 83	η_2'	-0.446×10^{-5}	η_3'	$0.030\ 9\times10^{-5}$
Y_o'	$0.190\ 0\times10^{-5}$	$Y_{\dot{e}^3}'$	−0.001 850		–
C_R'	0.002 26	m'	0.018 1		–

The mathematical relationships proposed by Fossen (2011) offer a means to quantitatively determine the influence of wave and wind effects on a ship by calculating the associated environmental forces and moments. These relationships incorporate various factors such as wave spectrum, wave kinematics, wind velocity, wind direction, vessel heading, vessel speed, and vessel size and shape. By utilising these relationships, one can estimate the magnitude and direction of the forces and moments acting on the vessel, thereby predicting their impact on the ship's manoeuvrability. This approach presents a viable alternative to employing computationally intensive computational fluid dynamics (CFD) models for assessing environmental forces and moments.

Notably, in Aydın et al. (2022), the authors focus on estimating environmental loads for dynamic positioning (DP) systems used in offshore operations. These DP systems are essential for maintaining vessel position and heading in various environmental conditions, such as wind, waves, and currents (Hassani et al., 2017). The paper conducts a comparative analysis of semi-empirical methods and computational fluid dynamics (CFD) approaches, aiming to improve the accuracy of load assessments. It offers valuable insights into refining initial load estimates, making it a useful resource for those involved in offshore operations and DP capability analysis.

In addition to waves and wind, the influence of sea currents should be considered for a more comprehensive understanding of ship performance in realistic situations. According to Ferrari et al. (2012) and Zhou et al. (2020), sea currents can significantly impact a ship's navigation and control system, particularly in path-tracking regimes. This influence can result in undesired wobbling movements deviating from the intended path and significant overshoots. The reduced capability to track the intended path accurately increases operation time and costs. In specific critical missions such as bathymetry recording or mine detection, the negative effects of sea currents on path-tracking can even lead to mission failure. To gain a deeper understanding of the influence of sea currents on ship performance, it is recommended to consult the detailed findings and insights presented by Ferrari et al. (2012), Zhou et al. (2020), Armudi et al. (2017); and Chen (2018).

3.1 Wind forces and moment

The wind forces and moment in 3DOF for crude carrier ships based on (Fossen, 2011) can be calculated through the following equations:

$$X_{\text{wind}} = \frac{1}{7.6} C_X(\gamma_w)\rho_a V_w^2 A_{Fw} \tag{13}$$

$$Y_{\text{wind}} = -\frac{1}{7.6} C_Y(\gamma_w)\rho_a V_w^2 A_{Lw} \tag{14}$$

$$N_{\text{wind}} = -\frac{1}{7.6} C_N(\gamma_w)\rho_a V_w^2 A_{Lw} L_{oA} \tag{15}$$

A_{Fw}, A_{Lw}, and L_{oA}, are front ship projection area, and side area projection above the waterline and length overall. ρ_a is air density, and the term γ_w has belonged to the wind direction to the heading of the ship. This angle is illustrated in Figure 3. It should be noted that γ_w, and V_w are attack angle and wind velocity, respectively given by (Fossen, 2011). Additionally, u_w represents the V_w component aligned with the x-direction while v_w corresponds to the V_w component aligned with the y-direction. The mentioned variables are calculated as:

$$\gamma_w = \varphi - \beta - \pi \tag{16}$$

$$V_w = \sqrt{\left(u - u_w\right)^2 + \left(v - v_w\right)^2} \tag{17}$$

$$u_w = V_w \cos\left(\beta - \varphi\right) \tag{18}$$

$$v_w = V_w \sin\left(\beta - \varphi\right) \tag{19}$$

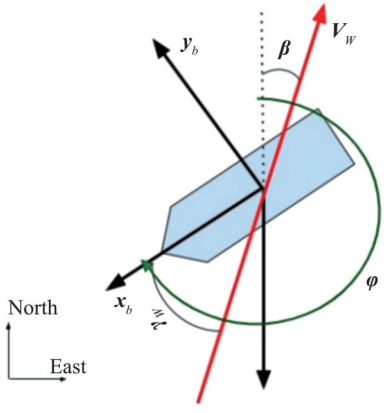

Figure 3 Wind speed V_w, direction β, angle of attack γ_w and ship's heading φ

The terms C_X, C_Y, and C_N represent wind coefficients and are calculated based on the angle of attack. As per (Fossen, 2011), these quantities are traditionally derived from specific plots for each parameter. However, for increased flexibility, an alternative approach involves fitting a polynomial to the graphs to obtain formulas that best represent the behaviour of each parameter as a function of the heading angle.

In this study, both the plots provided by Fossen (2011) and the regression toolbox of MATLAB have been utilised to calculate these three terms based on a more refined and accurate methodology:

$$\begin{aligned} C_X = {} & 1.865^{-12}\gamma^6 - 1.124^{-9}\gamma^5 + 2.511^{-7}\gamma^4 - 2.505^{-5}\gamma^3 \\ & + 0.001\,027\gamma^2 - 0.000\,315\,7\gamma - 0.866\,9 \end{aligned} \tag{20}$$

$$C_Y = -5.83^{-13}\gamma^6 + 3.684^{-10}\gamma^5 - 9.29^{-8}\gamma^4 + 1.139^{-5}\gamma^3 - 0.000\,532\,2\gamma^2 - 0.008\,086\gamma - 0.015\,08 \quad (21)$$

$$C_N = -1.154^{-9}\gamma^4 - 3.047^{-9}\gamma^3 + 6.16^{-5}\gamma^2 - 0.004\,379\gamma + 0.008\,646 \quad (22)$$

It should be noted that $\gamma = \gamma_w$ in Eq. 20 to Eq. 22 is in degree and is in the ranges of $0° \leqslant \gamma \leqslant 180°$.

3.2 Wave forces and moments

To expose the influence of the waves on the ship's motions, the first-order and second-order effects can be considered. The first-order effects based on (Fossen, 2011) are defined as wave-frequency motion observed as zero-mean oscillatory motions, and the second-order effect is wave drift forces observed as nonzero slowly varying components. In this study to simplify the procedure of calculating wind forces and moment in 3DOF, the linear model for first- and second-order wave-induced forces and moment is considered. In 3DOF motion, the forces and moment from the waves are given by (Fossen, 2011):

$$X_{\text{wave}} = \frac{K_w^{\{1\}} s}{s^2 + 2\zeta^{\{1\}} w_e^{\{1\}} s + \left(w_e^{\{1\}}\right)^2} w_1 + d_1 \quad (23)$$

$$Y_{\text{wave}} = \frac{K_w^{\{2\}} s}{s^2 + 2\zeta^{\{2\}} w_e^{\{2\}} s + \left(w_e^{\{2\}}\right)^2} w_2 + d_2 \quad (24)$$

$$N_{\text{wave}} = \frac{K_w^{\{6\}} s}{s^2 + 2\zeta^{\{6\}} w_e^{\{6\}} s + \left(w_e^{\{6\}}\right)^2} w_3 + d_3 \quad (25)$$

where the Wiener process is used to calculate the drift forces, d_i as:

$$\dot{d}_1 = w_4 \quad (26)$$

$$\dot{d}_2 = w_5 \quad (27)$$

$$\dot{d}_3 = w_6 \quad (28)$$

To adjust the amplitude of the wave forces and moment, $K_w^{\{\text{DOF}\}}$ are used. In Eq. 23 to Eq. 28, w is a white Gaussian noise which is used in simulation and $w_e^{\{\text{DOF}\}}$ are encounter frequency and ζ is a damping coefficient. In this research study $\zeta = 0.26$, based on the recommended value proposed in (Fossen, 2011). This value is implied when the Pierson–Moskowitz spectrum, S, is considered. This spectrum is utilised in this study.

The objective of the present study is to evaluate the performance of the designed controller under various sea states and ensure its robustness. To achieve this, the first five sea states are considered. The wave height ranges from 0.3 m to 3m, and the wind speed ranges from 1.5 m/s to 10.7 m/s. The focus on these particular sea states also ensures that the results are accurate and relevant to practical situations (Bitner-Gregersen et al., 2022; Lucas et al., 2011). Therefore, the study provides a comprehensive assessment of the controller performance and its ability to handle various sea states encountered in the area of interest.

After calculating the wind and wave forces and moments, the environmental effects on the mathematical model are calculated based on:

$$\chi_e = X_{\text{wave}} + X_{\text{wind}} \quad (29)$$

$$\Upsilon_e = Y_{\text{wave}} + Y_{\text{wind}} \quad (30)$$

$$H_e = N_{\text{wave}} + N_{\text{wind}} \quad (31)$$

This dynamic approach can enhance the adaptability and accuracy of the LoS guidance system, allowing it to respond more effectively to variations in the ship's position relative to the desired path.

To investigate and analyse the effect of environmental forces and moment on the motion, the simulation of the circular motion has been done by setting the rudder angle, δ, to its maximum value, $\delta = 35°$. Figure 4 illustrates the ship's trajectory in calm water and the presence of waves and wind. Compared to (Skejic and Faltinsen, 2013), the results reveal that the proposed procedure in calculating the environmental forces and moment effectively obtained for the 3DOF motions.

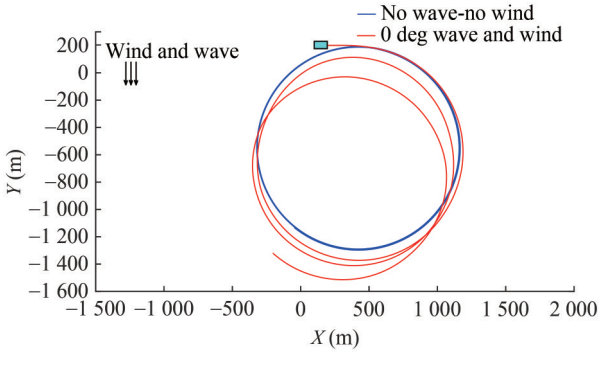

Figure 4 Ship trajectory in circular motion for calm water and 0° waves and wind.

4 Linear quadratic regulator (LQR) control strategy

Robustness and performance evaluation in the presence of waves and wind is a crucial process in designing autonomous ships. These disturbances need to be compensated differently by a control system (Fossen, 2011). The main goal of this research is to follow the predetermined path by

the ship. To achieve this goal, the controller based on the dynamic guidance system measures the desired angle according to its position and heading, and the corresponding rudder angle is determined to merge the ship reaching the desired path. The guidance system implemented in this research is described in the next subsection.

4.1 Guidance system

In the Line of Sight (LoS) guidance law, the main goal is to obtain the angle of inclination according to Figure 5 to force the ship to converge to the desired path. Two parameters have the greatest impact on the right angle for an autonomous ship to move toward the determined path. One of these parameters is the distance between the position coordinate of an autonomous ship or the control point and the path, e, and the other is the Δ. by obtaining these two parameters, it is possible to determine the $(x_{\mathrm{LoS}}, y_{\mathrm{LoS}})$. The distance between the control point and the path, e, can be easily determined using geometric equations, and the proposed function to achieve Δ is presented in

$$\Delta = L_{pp} e^{-0.25e} \tag{32}$$

The variable Δ plays a role in determining the LoS coordinates $(x_{\mathrm{LoS}}, y_{\mathrm{LoS}})$ as illustrated in Figure 5. Eq.32 describes how Δ is calculated dynamically based on the distance e. Instead of treating Δ as a constant value, it is calculated dynamically based on the distance of the ship from the desired path.

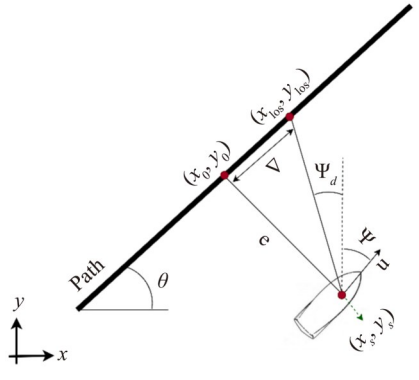

Figure 5 Guidance system

This dynamic calculation of Δ considers the changing position of the ship in relation to the desired path, which can be an improvement over a static or constant value.

Based on the Enclosure-Based Steering (Fossen, 2011), the desired angle for heading control to follow the defined path is given by:

$$\psi_d = \mathrm{atan2}\left(y_{\mathrm{LoS}} - y_s, x_{\mathrm{LoS}} - x_s\right) \tag{33}$$

4.2 First-order nomoto model

The first-order Nomoto model for steering is considered in this study to calculate the desired rudder angle based on the output of the guidance system. This model is widely used for autopilots (Moreira et al., 2007; Zhu et al., 2018; Xiao et al., 2012). The first-order Nomoto model for steering dynamic is described as:

$$\begin{aligned} \dot{\psi} &= r \\ T\dot{r} + r &= K\delta \end{aligned} \tag{34}$$

In this dynamic model K, and T are the Nomoto time and gain constant. Based on (Journée, 2001) these two parameters are calculated based on the zigzag manoeuvring test. The obtained values for these two parameters are as T = 24.285 2 s, K=0.016 0 s^{-1}.

4.3 Controller design

The LQR controller aims to find a rudder angle to minimise quadratic cost functions. The cost function considered in this research is presented in (Fossen, 2011) as:

$$J = \min\left\{\frac{0.007\,6}{Tf}\int_0^{Tf}\left(\varepsilon^2 + \lambda_1 r^2 + \lambda_2 \delta^2\right)\mathrm{d}t\right\} \tag{35}$$

where $\varepsilon = \psi - \psi_d$, and λ_1, and λ_2, are the weighting factors. To achieve optimal controller gains, three criteria as proposed by (Fossen, 2011) are used: Van Amerongen and Van Nauta Lemke's Steering (1978), Koyama (1967), and Norrbin (1972) criteria. Van Amerongen and Van Nauta Lemke's Steering criterion suggests that the control law should be proportional to the path following error, yaw rate, and the square of the yaw rate. Hence, based on the Steering criterion and the cost function, the control law should have the form:

$$\delta = -K_p\left(\psi - \psi_d\right) - K_d r \tag{36}$$

When designing a PD controller, the cost function J is minimised by adjusting the controller gains K_p and K_d. To achieve this, LQR control design method is used. The LQR problem involves solving the algebraic Riccati equation, which is a necessary condition for the optimality of the controller. In this problem, if the state used in this problem is considered as $[\varphi, r]$, the Riccati equation associated with the LQR problem is given by:

$$\begin{aligned} &\boldsymbol{A}^{\mathrm{T}}\boldsymbol{P} + \boldsymbol{P}\boldsymbol{A} - \boldsymbol{P}\boldsymbol{B}\boldsymbol{R}^{-1}\boldsymbol{B}^{\mathrm{T}}\boldsymbol{P} + \boldsymbol{Q} = 0 \\ &\boldsymbol{A} = \begin{bmatrix} 0 & 1 \\ 0 & -\dfrac{1}{T} \end{bmatrix}, \boldsymbol{B} = \begin{bmatrix} 0 \\ \dfrac{K}{T} \end{bmatrix}, \boldsymbol{Q} = \begin{bmatrix} 0 & 0 \\ 0 & \lambda_1 \end{bmatrix}, \boldsymbol{R} = \lambda_2 \end{aligned} \tag{37}$$

where $\boldsymbol{A}$, $\boldsymbol{B}$, $\boldsymbol{Q}$, and $\boldsymbol{R}$, are the state-space and weighting matrices, respectively, and $\boldsymbol{P}$ is the solution to the Riccati

equation, which is a symmetric positive definite matrix. The optimal feedback gain matrix $\boldsymbol{K}$ is then given by:

$$\boldsymbol{K}_{\mathrm{LQR}} = \boldsymbol{R}^{-1}\boldsymbol{B}^{\mathrm{T}}\boldsymbol{P} \tag{38}$$

substitute the expressions for $\boldsymbol{R}$, $\boldsymbol{B}$, and $\boldsymbol{P}$:

$$\boldsymbol{K}_{\mathrm{LQR}} = \lambda_2{}^{-1}\frac{\boldsymbol{K}}{T}\boldsymbol{P} \tag{39}$$

As a result, leveraging the matrices $\boldsymbol{A}$, $\boldsymbol{B}$, $\boldsymbol{Q}$, $\boldsymbol{R}$, and the Riccati equation (Eq. 37), the analysis performs matrix substitution to solve for the symmetric positive definite matrix $\boldsymbol{P}$. Subsequently, upon obtaining the solution for $\boldsymbol{P}$, the controller gains are determined following Eq.39.

$$K_p = \sqrt{\frac{1}{\lambda_2}} \tag{40}$$

$$K_d = \frac{\sqrt{1 + 2K_pKT + K^2\left(\lambda_1/\lambda_2\right)} - 1}{K} \tag{41}$$

The cost function, Eq. 35, includes the term $\lambda_2\,\delta^2$. To minimise this term, K_p should be inversely related to λ_2. As λ_2 increases (indicating higher cost associated with control effort), K_p should decrease to reduce the impact of the control input on the cost function. In proportional control law, the control input δ is proportional to the error ε (the difference between the desired and actual state). To minimise δ^2, a smaller K_p is needed when λ_2 is large. The choice of $1/\sqrt{\lambda_2}$ is made because it reflects an appropriate balance between error tracking and control effort. The square root relation ensures that as λ_2 increases, K_p decreases to put less emphasis on minimising δ^2 while still providing sufficient control to track the desired state. The specific formulation of K_d in this manner is a result of optimisation and control theory principles aimed at achieving a desired control response while balancing the trade-offs between tracking performance and control effort (Bitner-Gregersen et al., 2016). It reflects a design choice that is influenced by the system dynamics and control objectives.

The Koyama and Norrbin criterion for this system is obtained when $\lambda_1 = 0$ and $\lambda_2 = \lambda$. In this regard:

$$K_p = \sqrt{\frac{1}{\lambda}} \tag{42}$$

$$K_d = \frac{\sqrt{1 + 2K_pKT} - 1}{K} \tag{43}$$

Therefore, based on the mentioned criteria, according to the manoeuvre, λ should be determined according to the best performance considering the path following error, convergence to the desired path duration, and heading behaviour of the ship.

5 Optimal controller gains

When discussing autonomous ships, it is important to consider their manoeuvring performance and other constraints, such as reducing operation time to minimise fuel consumption. The controller proposed in this research study aims to achieve optimal performance by adjusting the control gain. The study considers environmental factors such as waves and wind that can significantly affect the ship's manoeuvrability. To determine the characteristics of ship manoeuvres under various sea conditions, the study employs different criteria and obtains optimal gains. Overall, the section focuses on developing an approach that can effectively handle the complex and dynamic nature of ship manoeuvres in varying environmental conditions.

To determine the optimal performance of the ship, four criteria are considered as follows:

• The evaluation of ship manoeuvring performance involves several criteria, one of which is the maximum deviation from the initial position, Δp. This criterion is important in cases where route limitations, such as canals, are present. The cross-check error from the initial position is calculated by changing the controller gain, λ, and the maximum cross-check error is used to obtain the best controller gain. The choice of the controller gain constant (λ) directly influences the ship's ability to maintain a precise course. Higher values of λ lead to more aggressive control responses, reducing Δp by promptly correcting deviations. Conversely, lower λ values result in smoother control actions but may lead to larger deviations from the initial position. The optimisation process seeks to find the λ value that minimises Δp while meeting other control objectives. By adjusting λ, the controller aims to strike a balance between rapid error correction and minimising deviations from the initial position. Thus, optimising λ ensures that the ship navigates precisely within constrained routes like canals.

• Another parameter used to assess the effectiveness of the manoeuvring controller is the maximum reaching time for the desired path, t_r. This criterion is determined by computing the cross-check error from the desired path, whereby the time corresponding to when the cross-check error reaches zero is recorded as the reaching time. λ plays a pivotal role in determining how quickly the ship reaches its intended path. Higher λ values result in more aggressive control actions, potentially leading to faster convergence and a shorter t_r. Conversely, lower λ values may lead to gentler control responses, extending t_r. The optimisation process aims to minimise t_r while considering other performance criteria. By adjusting λ, the controller seeks to find the balance between swift convergence and stable navigation. Optimising λ ensures that the ship efficiently follows the desired path and reaches its destination in minimum time.

• The third criterion considered in this research is the steady-state error, e_{ss}, which evaluates the distance between

the ship's path and the desired path under the influence of waves and wind. By adjusting λ, the control law can be fine-tuned to counteract the effects of disturbances. A well-optimised λ value allows the controller to actively mitigate deviations from the desired path, reducing e_{ss}. A higher λ typically results in a more aggressive response to disturbances, potentially leading to smaller e_{ss}values. To minimise e_{ss}, search for the λ value that minimises a cost function encompassing e_{ss} and other relevant criteria are conducted. This ensures that the ship maintains a precise trajectory along the desired path, even when confronted with external forces such as waves and wind.

• Finally, the last criterion is the maximum deviation of the heading compared to the desired value, $\Delta\psi$. This criterion is important in evaluating the performance of the thrust and rudder system and its relationship with fuel consumption. A minimum heading's overshot compared to the desired value is considered the optimal mode. These criteria provide a comprehensive evaluation of the performance of the ship manoeuvring controller under different environmental conditions. The parameter λ affects the control law that determines how the ship adjusts its heading in response to deviations from the desired course ($\Delta\psi$). A higher value of λ results in more aggressive heading corrections, reducing $\Delta\psi$ but potentially leading to overshooting the desired heading. Conversely, a lower λ leads to smoother heading adjustments but may result in slower response times and larger heading deviations. The goal is to find the optimal λ that strikes a balance between rapid heading corrections and minimising overshoot. This optimal value is obtained by minimising a cost function that incorporates criteria related to heading control, such as $\Delta\psi$. Thus, optimising λ ensures that the ship's heading remains closely aligned with the desired direction, enhancing the precision of its manoeuvres.

Considering the mentioned factors, in different sea states, sea state 1 to sea state 5, the performance of the proposed controller is evaluated and the optimal controller gain for each wave direction and sea state are obtained. The procedure to obtain the controller gain is done by minimising the cost function using the genetic algorithm technique. The cost function that is considered in this research is presented in:

$$C\left(t_r, \Delta p, \Delta\psi, e_{ss}\right) = \max\left(t_r\right) + \max\left(\Delta p\right) + \max\left(\Delta\psi\right) + e_{ss} \tag{44}$$

It should be noted that all mentioned parameters are normalised. The procedure of normalisation is described below.

The time the cross-check errors reach their steady-state error is noted and recorded. By taking this time as the maximum and 0 as the minimum, the reaching time is then normalised within this range. This normalisation process produces a value that falls between 0 and 1.

To normalise the ship's deviation from the initial point to reach the desired path, the distance between the initial point and the desired path is considered as a normalisation factor. This distance can be calculated as the shortest distance between the initial point and the desired path. By dividing the maximum deviation from the initial point by this distance, a normalised value between 0 and 1 is obtained, where 0 represents perfect performance (no deviation from the desired path), and 1 represents the worst performance (maximum deviation from the initial point).

To normalise the maximum heading overshoot of the ship from the desired heading, the following formula is used:

$$\max\left(\Delta\psi\right)_n = \frac{\max\left(\Delta\psi\right)}{\psi_d} \tag{45}$$

where n denotes the normalised value.

Eq.45 gives a value between 0 and 1, where 0 represents perfect performance (i. e., no overshoot) and 1 represents the worst performance (i.e., overshooting the desired heading by the full amount).

To normalise the steady-state error, the actual steady-state error is divided by the maximum allowable steady-state error (in this paper, the maximum allowable steady-state error is 10% of the ship's length):

$$e_{ss_n} = \frac{e_{ss}}{10\% \times L_{oA}} \tag{46}$$

The resulting value would be a normalised steady-state error between 0 and 1. The cost function, Eq. 44, is used in obtaining the optimal controller gain. The relationship between the two cost functions is as follows: Eq. 35 (J) is specifically used within the LQR controller design to optimise control gains by minimising the heading error and control input. However, the selection of λ is pivotal for achieving optimal performance and is determined through a separate criterion. To obtain the appropriate value for λ, attention turns to Eq. 44 (C), which serves as an overarching evaluation metric. Eq. 44 considers multiple criteria, including path following error, convergence to the desired path duration, and the heading behaviour of the ship, helping us identify the λ that best suits the desired performance under varying environmental conditions.

Genetic Algorithm (GA) is used to minimise the cost function and calculate the optimal controller gain. MATLAB optimisation toolbox is used. In the context of the genetic algorithm application, it is crucial to emphasise that the overarching objective is to fine-tune the controller gain parameter, denoted as λ, to optimise the autonomous ship's performance across various environmental conditions. λ plays a pivotal role in determining the ship's control strategy, influencing factors such as deviation from the initial position, reaching time for the desired path, steady-state error, and heading deviation. Higher values of λ tend to result in

more aggressive control responses, whereas lower values lean toward smoother, less aggressive responses. To ascertain the optimal λ value, the GA-based optimisation procedure systematically explores a range of potential solutions by evaluating their performance based on a composite cost function. This cost function takes into account multiple performance criteria, including path following error, convergence time, and heading behaviour. By iteratively selecting and evolving candidate solutions through genetic operations like crossover and mutation, the GA aims to converge towards the λ value that best aligns with the desired performance outcomes. Through these steps, we ensure that the ship's control system is adaptable and efficient, enabling precise manoeuvring even in the face of dynamic environmental challenges. Two criteria are considered for the stopping point in the genetic algorithm, the maximum number of generations and the plateau detection. For the maximum number of generations, a predetermined number of generations, 100 generations, is set as the maximum limit, and the algorithm stops when this limit is reached. For plateau detection, the algorithm stops when the cost function has remained unchanged for a specified number of generations. The range of control gain, λ, is defined as greater than 0, as it must be a positive value. The optimisation procedure is depicted in Figure 6, following a well-defined process:

• Initialisation: Begin with a set of controller weight λ and a population of candidate solutions.

• Evaluation: Evaluate the performance of each candidate solution using Eq. 43, which combines the various criteria for performance assessment.

• Selection: Select the top-performing candidate solutions based on their evaluation scores.

• Crossover and Mutation: Apply genetic operations such as crossover and mutation to create a new generation of candidate solutions.

• Termination Check: Check if termination criteria are met (the maximum number of generations and the plateau detection). If not, return to the Evaluation step.

• Optimal Solution: Once the optimisation process converges or reaches the maximum number of iterations, the optimal controller weight (λ) is determined based on the best-performing candidate solution.

6 Results and discussion

To determine the optimal controller gain for each sea state, waves and wind direction, a range of wave attack directions from −180° to 180° at 30° intervals are considered. The primary objective of the controller is to guide the ship towards the desired path. Figure 7 illustrates the desired path and the initial position of the ship, $\{(x_0, y_0, \psi_0) = (200\text{ m}, 200\text{ m}, 0°)\}$. Additionally, Figure 7 depicts the relative attack angle corresponding to the 0° waves and wind direction.

The primary aim of the proposed controller is to facilitate the convergence of the ship to the desired path. The controller accomplishes this by regulating the rudder angle in response to the desired heading, which is derived from the proposed dLoS approach while maintaining a constant surge speed. The controller gain for each of the 12 directional and 5 sea state scenarios are determined by manipulating a cost function proposed in Eq. 43 using GA. To gauge the effectiveness of the optimisation algorithm, the rate of convergence of the cost function to a minimum value is presented in Figure 8. As previously noted, the optimisation algorithm was subject to two constraints: a maximum

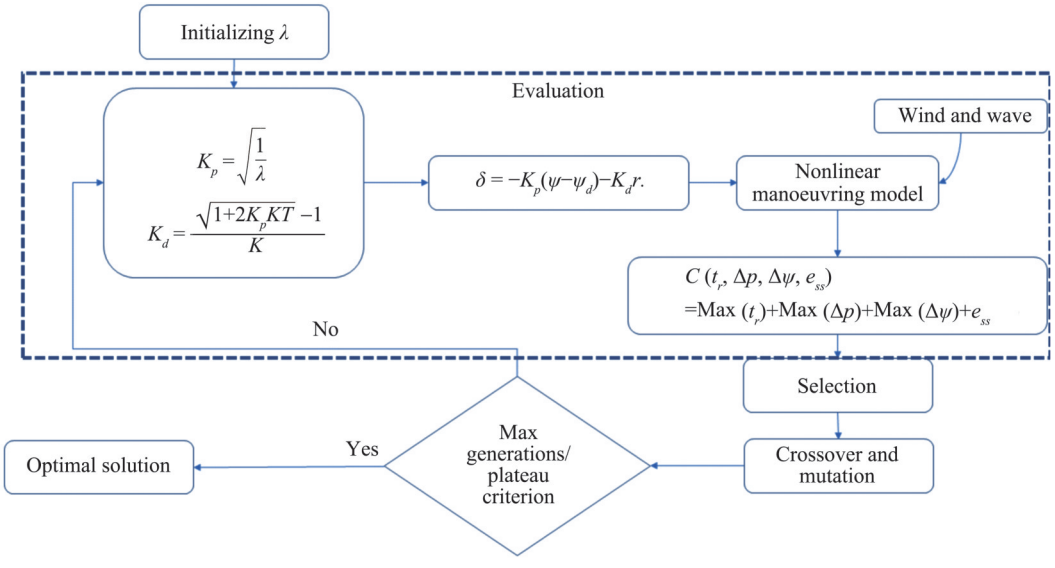

Figure 6 Optimisation procedure

number of generations (100 generations), and a plateau detection criterion. Examination of Figure 8 reveals that the algorithm terminated before completing 100 generations, implying activation of the latter constraint. The plot further demonstrates the algorithm's efficacy in reducing the cost function, with the resulting gains reflecting the controller's optimal performance as determined by the cost function's specifications.

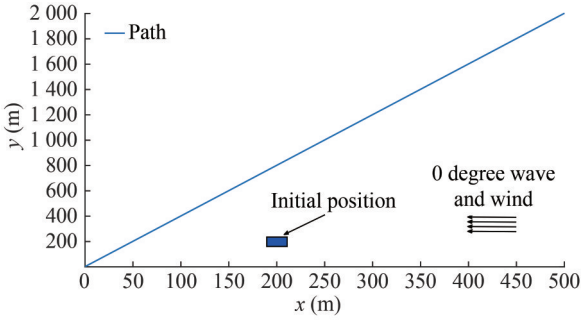

Figure 7 Desired path and initial condition of the ship

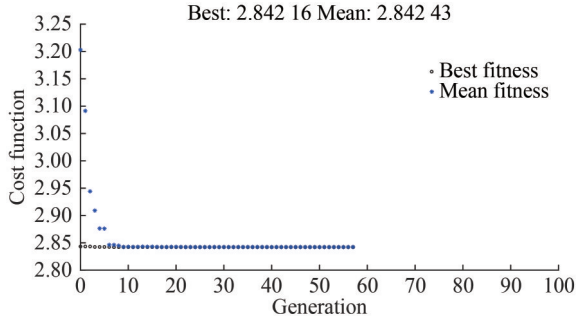

Figure 8 The optimisation algorithm performance

This study conducts a comprehensive analysis to optimise the gains for the LQR controller in various waves and wind directions. The optimisation process is carried out for all wave directions and sea states using a genetic algorithm. The obtained gains are then utilised in the proposed LQR controller to ensure that the ship can converge to the desired path accurately. The optimisation process results are presented in Figure 9, which demonstrates the optimal gains for different sea states and wave directions.

The results depicted in Figure 9 and Table 3 suggest that the controller gain for sea states 1 to 3 is not significantly different from those of calm water situations. These results indicate that the optimal controller gain for these sea states can be obtained by considering only the calm water situation. However, it is essential to note that the manoeuvring performance of the ship is directly correlated with the time it takes to complete the manoeuvre, and this directly impacts the financial cost. Moreover, the accuracy required for special situations also needs to be considered. Therefore, it is recommended that the effects of waves and wind disturbances in these sea states be incorporated to ensure efficient and accurate manoeuvring of the ship.

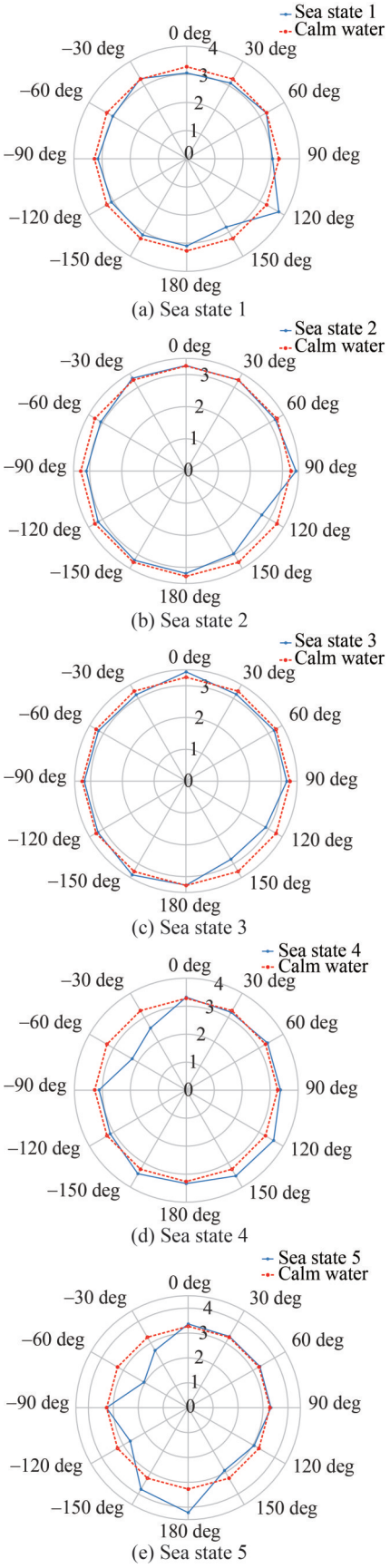

Figure 9 Optimal controller gain for different sea state

Table 3 Optimal control gains

Sea state	Wave and wind direction											
	−150	−120	−90	−60	−30	0	30	60	90	120	150	180
1	3.124 5	3.082 3	3.150 3	3.029 0	3.288 5	3.050 2	3.107 6	3.257 7	3.043 2	3.771 3	2.801 3	3.097 1
2	3.200 4	3.154 7	3.097 9	3.060 1	3.333 4	3.283 9	3.268 1	3.210 1	3.426 2	2.724 0	2.965 9	3.180 1
3	3.394 7	3.206 9	3.206 2	3.185 8	3.142 0	3.438 5	3.158 2	3.200 2	3.168 1	2.890 7	2.824 6	3.263 8
4	3.456 2	3.137 0	3.115 0	2.228 7	2.552 3	3.312 2	3.204 5	3.356 7	3.370 3	3.609 2	3.457 2	3.344 6
5	3.787 9	2.685 0	3.279 5	2.048 7	2.660 3	3.363 6	3.306 1	3.315 0	3.313 1	3.046 4	2.910 1	4.217 4

The results of the analysis in sea state 4 and sea state 5 demonstrate that the controller has a significant impact on the rudder angle in response to deviations from the desired heading in 180° wave direction, while lower controller gains in −60° and −30° directions indicate a weaker influence of the controller on the rudder angle for the same error signal.

These findings for −60° and −30° directions are reasonable due to the increased influence of waves and wind on ship performance during port turns, leading to reduced influence of the rudder angle.

The higher gains observed in the 180° wave direction compared to calm water suggest that the location of the desired path relative to the initial position of the ship, as well as the angle of the desired path to the *x*-axis, have a greater influence on ship performance in this direction, thus requiring the controller to work harder to maintain the ship heading. This effect is particularly significant in sea states over 3, where the characteristics of the waves and wind are more pronounced, and their impact on the ship is more powerful, especially considering the length and draft of the ship.

Based on data provided by the boxplot in Figure 10, the box plot shows the distribution of controller gain for different wave directions. The fact that the gains for all wave directions are distributed within a narrow range of 2.8 to 3.5 indicates that the controller can maintain stable performance across different waves directions.

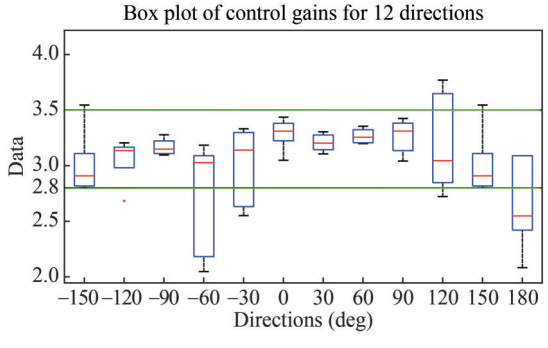

Figure 10 Controller gain distribution in different waves and wind directions

Furthermore, it is notable that the box sizes at 120°, −60°, and −30° are relatively larger. This observation can be attributed to various influencing factors. Specifically, the increased variability in controller gain for these wave directions is influenced by the complex interplay of factors, including the ship's response to wave and wind disturbances, the initial position and heading of the ship, and the angular relationship between the desired path and the *x*-axis.

The median of all boxes in Figure 10 are in the same range, which means that the central tendency of the data is similar across all waves directions. This suggests that the LQR controller gains perform consistently across different wave directions.

Based on the box plot in Figure 11, the data distribution for the case of waves and wind situations is more spread out than the calm water situation. The box plot also shows that the data is tightly distributed for the calm water situation, with no outliers. However, for the waves and wind situations, the range of the data is wider, indicating a greater variation in the controller gains across different sea states and waves directions. This suggests that the controller gain must be carefully tuned to account for the variations caused by waves and wind disturbances, especially in sea states above 3, to ensure optimal ship performance. After accounting for these factors, it becomes evident that the variability in controller gain for specific wave directions is a valuable insight into the adaptability of our control system. This adaptability ensures that our ship maintains stable performance even in challenging maritime conditions.

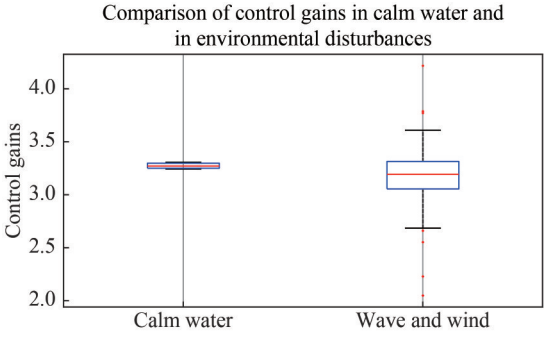

Figure 11 Distribution of the controller gain in calm water and environmental disturbances situation

After determining the control gain for various scenarios, the performance of the controller in following the desired

path is assessed through simulation under specific conditions. For this purpose, a waves direction of − 60° in sea state 3 is chosen. The obtained results are depicted in Figures 12 to 15, providing a visual representation of the controller performance evaluation.

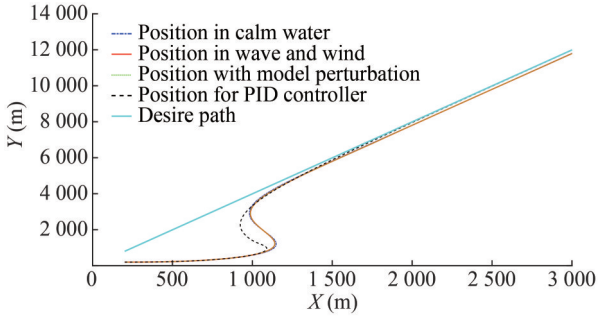

Figure 12 Ship trajectory in sea state 3 and waves direction −60°

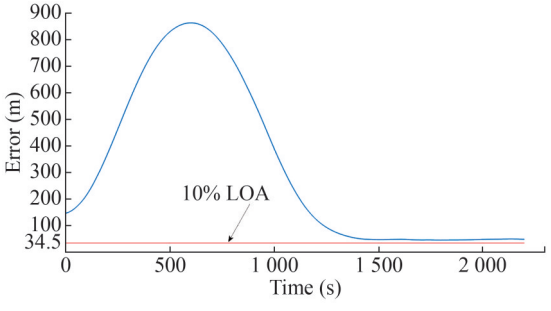

Figure 13 Cross-check error for the path following sea state 3, −60° waves and wind

For this situation, the optimal controller gain is determined using a comprehensive evaluation based on four different criteria, including the consideration of steady-state error. Subsequently, when applying the optimal controller to the simulation, it is observed that the ship exhibits a remarkable convergence towards the desired path. This convergence serves as evidence of the controller's effective performance in guiding the ship along the intended trajectory. However, it is important to note that despite the significant convergence, a steady-state error is observed (Figure 12). This indicates a persistent deviation between the actual path followed by the ship and the desired path, even after the controller has reached a steady-state condition.

On the other hand, comparing the results in Figure 12 reveals that, in the case of using a more practical and commercial controller like PID, the convergence of the ship to the desired path faces more agreement compared to LQR. It should be noted that even though this performance is more favourable compared to LQR, the overall decision on the evaluation should be made by considering other parameters, such as the rudder angle deflection, which will be discussed in more detail.

Upon plotting the cross-check error for the path following controller, Figure 13 shows that the steady-state error surpassed 10 per cent of the overall length of the ship. Despite this steady-state error, the convergence of the error can be deemed acceptable. The error diminishes over time and eventually stabilises, indicating that the ship follows the desired path closely.

Another aspect considered in this evaluation is the robustness of the controller. To achieve this goal, the simulation is also conducted for a specific condition when model perturbations occur. To create this situation, the yaw rate of the ship is exposed to white noise to generate a situation with a Signal-to-Noise Ratio of 14.172 1. From Figure 12, it can be concluded that even though this perturbation affects the process of controller design, the overall performance of the ship is not considerably influenced. On the other hand,

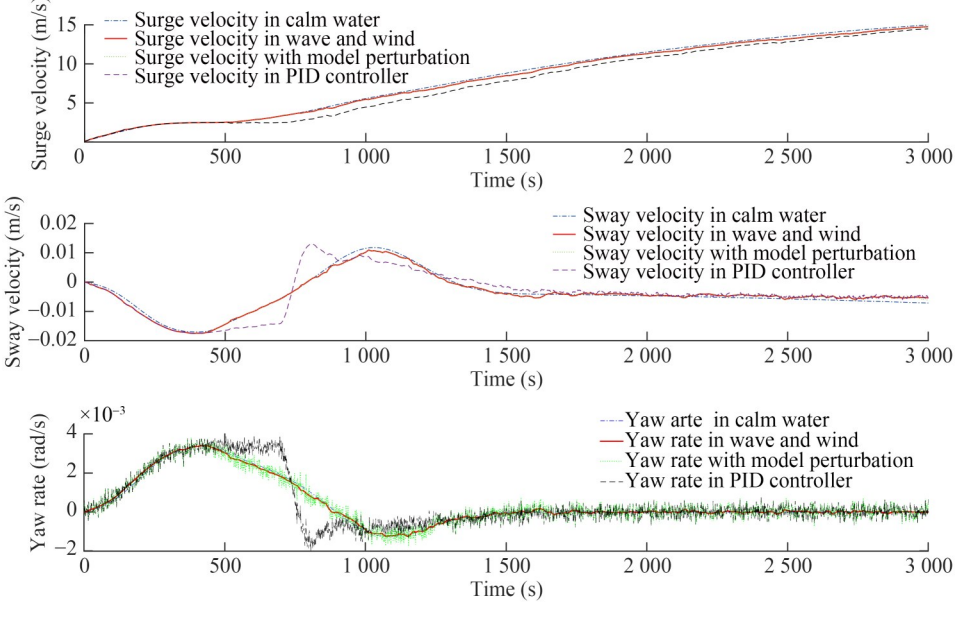

Figure 14 Velocity profiles during course correction amidst wave and wind disturbances

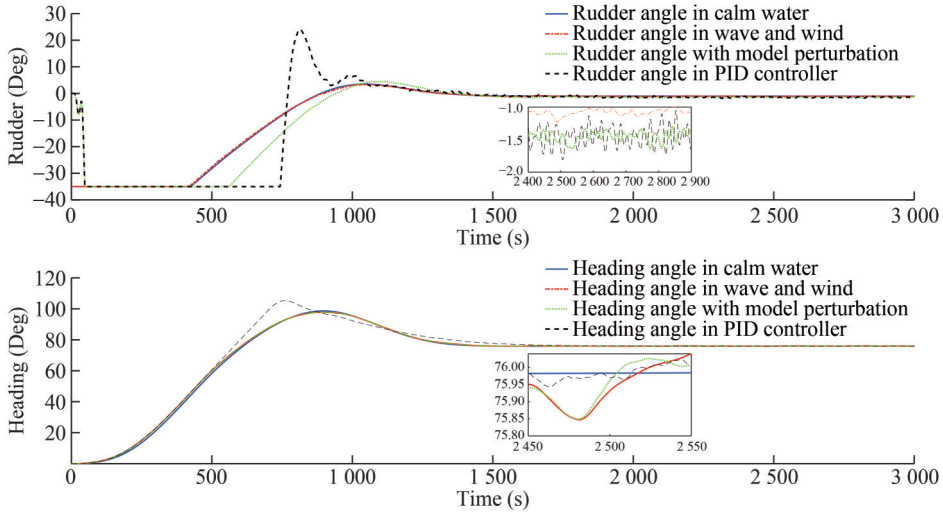

Figure 15 Heading and rudder angle time series

focusing solely on the path tracking of the ship without considering other parameters like the rudder angle (controller), no significant change appears. Hence, it could be concluded that even with model perturbation, the proposed controller performance is generally acceptable.

The observed trends in surge velocity (u) in Figure 14 provide valuable insights into the dynamic behaviour of the vessel during its course. Initially, as the vessel commences its journey, surge velocity starts from a standstill and smoothly increases. However, a notable point in this journey is when the vessel begins to adjust its course to align with the desired path. At this juncture, surge velocity exhibits a momentary steadiness before continuing its ascent. The final stabilisation of surge velocity at approximately 18 m/s coincides with a fixed propeller rotation speed of 1.35 r/min, signifying a steady-state condition. Importantly, the unsmooth behaviour of the graph during certain phases can be attributed to environmental disturbances, such as waves and wind, which momentarily influence the vessel's propulsion and stability. Sway velocity (v) in Figure 14 reflects the vessel's lateral motion and its response to manoeuvres and external forces. Initially, as the vessel navigates its course, sway velocity experiences fluctuations. These fluctuations are particularly pronounced during course changes, with sway velocity reaching its maximum value at such points. Upon reaching the desired path, sway velocity stabilises for a duration, indicating the vessel's lateral alignment with its intended trajectory. Nevertheless, over time, there is a decrease in sway velocity. This reduction can be attributed to the vessel's response to environmental factors, notably the angle of the desired path relative to the direction of waves and wind. The graph's unsmooth behaviour is indicative of the vessel's adaptability to mitigate environmental sway disturbances.

The yaw velocity (r) graph in Figure 14 provides insights into the vessel's rotational behaviour and its ability to maintain a consistent heading angle. Initially, yaw velocity changes as the vessel adjusts its course. However, once the vessel reaches its desired path, the yaw velocity experiences minor deviations around zero. While seemingly irregular, these deviations reveal the controller's effectiveness in counteracting disturbances from the sea environment. Despite the presence of external forces, the vessel's heading angle remains remarkably stable. This outcome underscores the success of the controller's primary objective, which was designed to precisely maintain the vessel's heading angle based on the desired path. In sum, the unsmooth behaviour of the yaw velocity graph signifies the vessel's resilience against environmental perturbations, showcasing the controller's robust performance in maintaining course direction.

Both situations of utilising the PID controller and considering model perturbation are presented in Figure 14. Evaluating the results in this context reveals that the surge velocity, due to the model perturbation and the use of the PID controller, does not significantly change the outcome. Hence, these parameters may not be the best options for analysing the robustness and the advantages of the proposed controller over PID. However, looking at sway velocity in all cases along with yaw rate changes uncovers the advantage of the proposed controller over PID.

Figure 14 reveals that the smoothness of the results in all cases except the PID controller is more evident. Hence, it can be said that the performance of the controller and the system is more stable in the proposed controller compared to PID. That might not be a perfect comparison; however, less change in practice is always favourable.

To evaluate the performance of the controller, an analysis focusing on two pivotal parameters is conducted: the ship's heading angle and its corresponding rudder angle, as depicted in Figure 15. The empirical data presented in the figures unequivocally illustrates the ship's heading angle exhibiting a convergent behaviour towards the intended direction within a finite timeframe. This convergent ten-

dency in the heading angle signifies the controller's effectiveness in guiding the vessel along the desired trajectory.

Notably, the heading angle is assessed under varying environmental conditions, including both calm water scenarios and situations influenced by waves and wind forces. Figure 15 elucidates that environmental forces, such as waves and wind, introduce significant delays in achieving the desired heading. Furthermore, the convergence rate towards the intended heading exhibits non-smooth behaviour, attributed to the stochastic nature of waves and wind patterns.

Regarding the rudder angle, it exhibited dynamic changes over time to facilitate the convergence of the ship to the desired path. The variations in the rudder angle reflected the controller's continuous adjustments in response to external disturbances, varying sea conditions, and deviations from the desired path. By modulating the rudder angle, the controller effectively guided the ship along the desired trajectory, compensating for any deviations and ensuring course correction towards the intended path.

Along with the previous parameters regarding the performance of the proposed controller, when looking at the controller output in more detail, it is clear that the smoothness of the LQR controller in maintaining the ship positions along the desired path is evident. Rudder deviation, even after applying a lowpass filter to the controller output in the PID controller, is more than the controller output of the proposed LQR. Hence, it could be concluded that, although solely looking at the position of the ship may suggest that PID performs better than the proposed LQR, a more detailed investigation into the controller commands, which directly influence the performance of the actuator, reveals that PID, due to the higher deviation range compared to the proposed LQR, is not the best option and may lead to an increase in maintenance costs.

To elucidate the discernible divergence between the conditions of calm water and those influenced by waves and wind dynamics, we have generated graphical representations of the surge and sway forces, as presented in Figure 16. A noteworthy observation from this figure is that the ship undergoes a significant course change, resulting in a marked elevation of the forces. It is discernible from the force magnitudes that, following the waves' direction, the ship is subjected to higher environmental forces. Consequently, the associated delay in the rudder angle's return to its equilibrium position during this manoeuvre can be deemed justifiable.

This phenomenon is also reflected in the behaviour of the heading angle. Due to the perturbations induced by waves and wind interactions, the heading angle experiences a delay in attaining its desired value when compared to the scenario of calm water conditions. Furthermore, this trend exhibits non-smooth characteristics, indicative of these environmental factors' unpredictable and fluctuating nature.

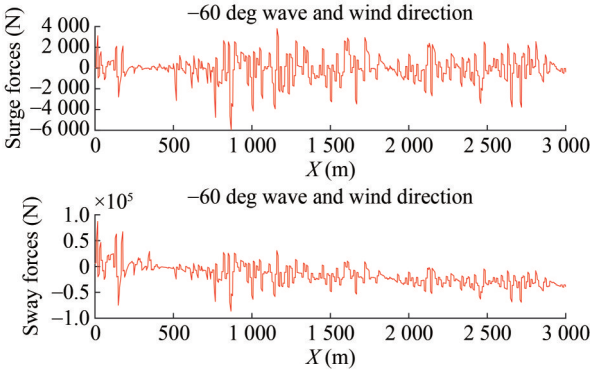

Figure 16 Ship confronts surge and sway in the face of -60° wave and wind forces

7 Conclusions

The study focuses on optimising the controller gains for various sea states, as well as wave and wind directions. The proposed controller demonstrates the ability to guide the ship towards the desired path by regulating the rudder angle based on the dynamic Line of Sight approach. The optimisation process, facilitated by a genetic algorithm, successfully determined the optimal gain for different scenarios, ensuring accurate path following.

The significance of optimal control gain under various sea state conditions, encompassing scenarios ranging from calm waters to wavy conditions, was thoroughly discussed. This discussion, particularly, sheds light on how the presence of waves and wind can impact controller performance. The analysis of the optimisation results revealed that for sea states 1 to 3, the controller gains are not significantly different from those in calm water situations. This implies that considering only calm water conditions might be sufficient to obtain optimal gains for these sea states. However, to ensure efficient and accurate manoeuvring, it is recommended to incorporate the effects of waves and wind disturbances in these sea states. The analysis also highlighted the influence of waves and wind conditions on the ship's performance, particularly in sea states above 3. The controller gains exhibited significant variations depending on the waves direction, indicating the impact of the desired path's location relative to the ship's initial position and heading. It was observed that the controller exerted more influence on the rudder angle in response to deviations from the desired heading in certain wave directions while exhibiting weaker influence in others due to the increased influence of waves and wind disturbances during specific manoeuvres.

Similarly, the proposed controller demonstrates robustness to perturbations, as evidenced by its stable performance even under model disturbances. Overall, it outperforms the classical PID controller, exhibiting smoother controller output and lower actuator deviations, highlight-

ing its superior efficiency in maritime control applications.

The box plots provide insights into the distribution of controller gains across different wave directions and sea states. The consistent range of gains suggested the stable performance of the controller, while the larger box sizes for certain wave directions indicated higher variability. These variations can be attributed to factors such as the ship's response to waves and wind disturbances and the alignment of the desired path with the ship's initial position and heading.

Path-following simulation results illustrated the controller performance in following the desired path under specific conditions. A steady-state error was observed while the ship exhibited remarkable convergence towards the desired path. Despite this error, the convergence of the error was deemed acceptable, as it diminished over time and stabilised. The analysis of the heading angle and rudder angle plots further supported the successful guidance of the ship towards the intended direction, with dynamic adjustments made to ensure accurate path following.

The study successfully optimised the controller gains for path-following in various sea states, wave directions, and wind conditions. The analysis revealed the influence of these factors on the controller performance, emphasising the need for careful tuning of gains to account for waves and wind disturbances. The results demonstrated the effectiveness of the controller in guiding the ship towards the desired path, although steady-state errors and variations in controller gains were observed. Further research can focus on refining the control strategy to minimise steady-state errors and enhance the controller performance under varying environmental conditions.

Funding This work is financially supported by the Portuguese Foundation for Science and Technology (Fundação para a Ciência e Tecnologia-FCT), and it contributes to the Strategic Research Plan of the Centre for Marine Technology and Ocean Engineering (Grant No. UIDB/UIDP/00134/2020). The FCT has also funded the first author for his doctoral fellowship (Grant No. 2023.03496.BD).

Competing interest C. Guedes Soares is one of the Editors for the Journal of Marine Science and Application and was not involved in the editorial review, or the decision to publish this article. All authors declare that there are no other competing interests.

References

Abkowitz MA (1980) Measurement of hydrodynamic characteristics from ship manoeuvring trials by system identification. Transactions of Society of Naval Architects and Marine Engineers, 88: 283-318

Armudi A, Marques WC, Oleinik PH (2017) Analysis of ship behavior under influence of waves and currents. Revista de Engenharia Térmica. 16(2): 18. https://doi.org/10.5380/reterm.v16i2.62206

Astolfi A, Karagiannis D, Ortega R (2007) Non-linear and Adaptive Control with Applications. Springer London

Aung MZ, Umeda N (2020) Manoeuvring simulations in adverse weather conditions with the effects of propeller and rudder emergence taken into account. Ocean Eng. 197, 106857. https://doi.org/10.1016/j.oceaneng.2019.106857

Aydın Ç, Ünal UO, Sarıöz K (2022) Computation of environmental loads towards an accurate dynamic positioning capability analysis. Ocean Eng. 243, 110201

Bali A., Singh UP, Kumar R, Jain S (2024) Neural Networks Based-Adaptive Control of Non-linear Ship Manoeuvring System. J Control Autom Electr Syst 35, 314-325

Banazadeh A, Ghorbani MT (2013) Frequency domain identification of the Nomoto model to facilitate Kalman filter estimation and PID heading control of a patrol vessel. Ocean Eng. 72, 344-355. https://doi.org/10.1016/j.oceaneng.2013.07.003

Bitner-Gregersen EM, Guedes Soares C, Vantorre M (2016) Adverse weather conditions for ship manoeuvrability. Transp. Res. Proc. 14, 1631-1640. https://doi.org/10.1016/j.trpro.2016.05.128

Bitner-Gregersen EM, Waseda T, Parunov J, Yim S, Hirdaris S, Ma N, Guedes Soares C (2022) Uncertainties in long-term wave modelling. Mar. Struct. 84, 103217. https://doi.org/10.1016/j.marstruc.2022.103217

Boyd S, Vandenberghe L (2004) Convex Optimization. Cambridge: Cambridge University Press

Cai Z, He C, Liu X, Chen W (2023) On the wave height distribution of waves and wave packets around a reef lagoon of the South China Sea. Ocean Eng. 269, 113560. https://doi.org/10.1016/j.oceaneng.2022.113560

Chen C (2018) Case study on wave-current interaction and its effects on ship navigation. J Hydrodyn. 30: 411-419. https://doi.org/10.1007/s42241-018-0050-5

Chen G, Yin J, Yang S (2023) Ship autonomous berthing simulation based on covariance matrix adaptation evolution strategy. J. Mar. Sci. Eng. 11, 1400. https://doi.org/10.3390/jmse11071400

Chen Q, Yang J, Mao J, Liang Z, Lu C, Sun PA (2023) Path following controller for deep-sea mining vehicles considering slip control and random resistance based on improved deep deterministic policy gradient. Ocean Eng. 278, 114069. https://doi.org/10.1016/j.oceaneng.2023.114069

Codesseira VC, Tannuri EA (2021) Path following control for autonomous ship using model Predictive Control. IFAC-PapersOnLine. 54(16): 57-62. https://doi.org/10.1016/j.ifacol.2021.10.073

Das S, Talole SE, (2015). Effect of Environmental Disturbances on Marine Surface Vessels. MILIT J. 4, 21-26

Deng Y, Zhang X, Im N, Zhang G, Zhang Q (2020) Model-based event-triggered tracking control of underactuated surface vessels with minimum learning parameters. IEEE Transactions on Neural Networks and Learning Systems, 31(10): 4001-4014

Du W, Li Y, Zhang G, Wang C, Chen P, Qiao J (2021) Estimation of ship routes considering weather and constraints. Ocean Eng. 228, 108695. https://doi.org/10.1016/j.oceaneng.2021.108695

Feng X, Xiao T, Xing X, Liu Z (2014) Identification of Nomoto models with integral sample structure for identification. In Proceedings of the 33rd Chinese Control Conference China, 6721-6725. https://doi.org/10.1109/ChiCC.2014.6896105

Ferrari V, Moreira L, Sutulo S, Guedes Soares C (2012) Influence of sea currents on manoeuvring of a surface autonomous model. In Guedes Soares C, Garbatov Y, Sutulo S, Santos TA Eds. Maritime Engineering and Technology, 173-180. London, UK: Taylor & Francis Group

Fossen TI (2011) Handbook of marine craft hydrodynamics and motion control. John Wiley and Sons, Ltd

Ghassemzadeh A, Xu H, Guedes Soares C (2023) Path following

control using robust sliding mode for an autonomous surface vessel based on ε- support vector regression identified steering model. Ocean Engineering, 288, 116085. https://doi.org/10.1016/j.oceaneng.2023.116085

Hassani V, Sørensen AJ, Pascoal AM, Athans M (2017) Robust dynamic positioning of offshore vessels using mixed-μ synthesis modeling, design, and practice. Ocean Eng. 129, 389-400

Hinostroza MA, Xu H, Guedes Soares C (2018) Path-planning and path-following control system for autonomous surface vessel. In Maritime Transportation and Harvesting of Sea Resources; Guedes Soares C, Teixeira AP, Eds. Taylor & Francis Group, London, UK, 991-998

IMO (2021) Guidance for determining minimum propulsion power to maintain the Maneuverability of ships in adverse condition. MEPC.1/Circ.850/Rev.3

ITTC (2000) General 1.1. Membership and Meetings. Proceedings of the 23rd ITTC. Vol II

Jafari M, Vatani A, Salarieh H (2018) Maneuvering control of a marine surface vessel using a non-linear feedback controller. J. Mar. Sci. Appl. 17(2): 237-245

Jiang X, Xia G (2022) Sliding mode formation control of leaderless unmanned surface vehicles with environmental disturbances. Ocean Eng. 244, 110301. https://doi.org/10.1016/j.oceaneng.2021.110301

Journée J (2001) A simple method for determining the manoeuvring indices K and T from zigzag trial data. Ship Hydromechanics Laboratory, Delft University of Technology, Netherlands

Kim D (2018) Estimation of hydrodynamic coefficients from results of real ship sea trials. Polish Maritime Research. 25, 65-72

Kim DJ, Yun K, Park JY, Yeo DJ, Kim YG (2019) Experimental investigation on turning characteristics of KVLCC2 tanker in regular waves, Ocean Eng. 175, 197-206, 0029-8018. https://doi.org/10.1016/j.oceaneng.2019.02.011

Kim DJ, Choi H, Yun K, Yeo DJ, Kim YG (2022) Experimental study on turning characteristics of KVLCC2 tanker in long-crested irregular waves. Ocean Eng. 244, 110362. https://doi.org/10.1016/j.oceaneng.2021.110362

Kim D, Tezdogan T (2022) CFD-based hydrodynamic analyses of ship course keeping control and turning performance in irregular waves. Ocean Eng. 248, 110808. https://doi.org/10.1016/j.oceaneng.2022.110808

Koyama T (1967) On the optimum automatic steering system of ships at sea. Journal of Zosen Kiokai. 1967(122):18-35

Lan J, Zheng M, Chu X, Ding S (2023) Parameter prediction of the non-linear Nomoto model for different ship loading conditions using support vector regression. J. Mar. Sci. Eng. 11(5). https://doi.org/10.3390/jmse11050903

LeCun Y, Bengio Y, Hinton G (2015) Deep learning. Nature 521, 436-444

Li G, Zhang X (2022) Research on the influence of wind, waves, and tidal current on ship turning ability based on Norrbin model. Ocean Eng. 259, 111875. https://doi.org/10.1016/j.oceaneng.2022.111875

Li Y (2004) The simulation of ship maneuvering and course keeping with escort tug. Master dissertation. The University of British Columbia

Li Z, Li R, Bu R (2021) Path following of under-actuated ships based on model predictive control with state observer. JASNAOE. 26, 408-418. https://doi.org/10.1007/s00773-020-00746-1

Lucas C, Boukhanovsky A, Guedes Soares C (2011) Modeling the climatic variability of directional wave spectra. Ocean Eng. 38(11), 1283-1290. https://doi.org/10.1016/j.oceaneng.2011.04.003

Ma C, Hino T, Ma N, Takagi Y (2022) CFD investigation on the hydrodynamic loads and motions when ship maneuvers in regular and irregular waves. Ocean Eng. 266, 113040. https://doi.org/10.1016/j.oceaneng.2022.113040

McTaggart KA (1992) Wind effects on intact ship stability in beam seas. J. Wind. Eng. Ind. Aerodyn. 44(1): 2487-2498. https://doi.org/10.1016/0167-6105(92)90040-H

McTaggart K (2008) Improved maneuvering forces and autopilot modelling for the ShipMo3D Ship Motion Library. Defence Research and Development Canada.162

Mei B, Sun L, Shi G (2020) Full-scale maneuvering trials correction and motion modelling based on actual sea and weather conditions. Sensors. 20, 3963. https://doi.org/10.3390/s20143963

Min B, Zhang X (2021) Concise robust fuzzy non-linear feedback track keeping control for ships using multi-technique improved LOS guidance. Ocean Eng. 224, 108734. https://doi.org/10.1016/j.oceaneng.2021.108734

Moreira L, Fossen TI, Guedes Soares C (2007) Path following control system for a tanker ship model. Ocean Eng. 34(14): 2074-2085. https://doi.org/10.1016/j.oceaneng.2007.02.005

Neary VS, Ahn S (2023) Global atlas of extreme significant wave heights and relative risk ratios. Renewable Energy. 208: 130-140. https://doi.org/10.1016/j.renene.2023.03.079

Norrbin NH (1972) On the added resistance due to steering on a straight course. In: Proceedings of the 13th ITTC. Berlin, Hamburg, Germany

Qu X, Jiang Y, Zhang R, Long F (2023) A deep reinforcement learning-based path-following control scheme for an uncertain under-actuated autonomous marine vehicle. Journal of Marine Science and Engineering, 11(9): 1762

Ren RY, Zou ZJ, Wang Y D, Wang XG (2018) Adaptive Nomoto model used in the path following problem of ships. J. Mar. Sci. Technol. 23(4): 888-898. https://doi.org/10.1007/s00773-017-0518-y

Ren Y, Zhang L, Huang W, Chen X (2023) Neural network-based adaptive sigmoid circular path-following control for underactuated unmanned surface vessels under ocean disturbances. Journal of Marine Science and Engineering, 11(11): 2160

Ribeiro MT, Singh S, Guestrin C (2016) Why should i trust you? Explaining the predictions of any classifier. Proceedings of the 22nd ACM SIGKDD International Conference on Knowledge Discovery and Data Mining

Sayyaadi H, Ghassemzadeh A (2018) Control of multiple underwater vessels to converge to a desired pattern. International Journal of Maritime Technology, 9(1): 51-57. https://doi.org/10.29252/ijmt. 9.51

Schmidhuber J (2015) Deep learning in neural networks: an overview. Neural Networks, 61: 85-117

Seo MG, Nam BW, Kim YG (2019) Numerical evaluation of ship turning performance in regular and irregular waves. J. Offshore Mech. Arct. Eng. 142(2). https://doi.org/10.1115/1.4045095

Skejic R, Faltinsen OM (2013) Maneuvering behavior of ships in irregular waves. Proceedings of the ASME 32nd International Conference on Ocean, Offshore and Arctic Engineering. Nantes, France, 9: 9-14

Sutton RS, Barto AG (2018) Reinforcement learning: An introduction. 2nd ed. The MIT Press

Sutulo S, Guedes Soares C (2011) Mathematical models for simulation of manoeuvring performance of ships. In Guedes Soares C, Garbatov Y, Fonseca N, Teixeira AP Eds. Marine Technology and Engineering, 661-698. London, UK: Taylor & Francis Group

Sutulo S, Guedes Soares C (2024) Nomoto-type manoeuvring mathematical models and their applicability to simulation tasks.

Ocean Engineering, 117639. https://doi.org/10.1016/j.oceaneng.2024.117639

Terada D, Matsuda M (2023) On rudder-roll stabilisation autopilot based on response models. Ocean Eng. 272, 113869. https://doi.org/10.1016/j.oceaneng.2023.113869

Tiwari K, Krishnankutty P (2021) Comparison of PID and LQR controllers for dynamic positioning of an oceanographic research vessel. In: Sundar V, Sannasiraj SA, Sriram V, Nowbuth MD, eds. Proceedings of the Fifth International Conference in Ocean Engineering (ICOE2019). Lecture Notes in Civil Engineering, vol 106. Springer, Singapore. https://doi.org/10.1007/978-981-15-8506-7_28

Van Amerongen J, Van Nauta Lemke HR (1978) Optimum steering of ships with an adaptive autopilot. In: Proceedings of the 5th Ship Control Systems Symposium. Annapolis, USA

Vettor R, Guedes Soares C (2015) Detection and analysis of the main routes of voluntary observing ships in the North Atlantic. Journal of Navigation. 68(2): 397-410

Woo J, Yu C, Kim N (2019) Deep reinforcement learning-based controller for path following of an unmanned surface vehicle. Ocean Eng. 183, 155-166. https://doi.org/10.1016/j.oceaneng.2019.04.099

Xiao L, Fossen TI, Jouffroy J (2012) Non-linear robust heading control for sailing yachts. IFAC Proceedings, 45(27): 404-409. https://doi.org/10.3182/20120919-3-IT-2046.00069

Xu H, Guedes Soares C (2016a) Vector field path following for surface marine vessel and parameter identification based on LS-SVM. Ocean Eng. 113, 151-161.

Xu H, Guedes Soares C (2016b) Waypoint-following for a marine surface ship model based on vector field guidance law. In Maritime Technology and Engineering 3; Guedes Soares C, Santos TA, Eds.; Taylor & Francis Group: London, UK. Vol 1, 409-418

Xu H, Hassani V, Guedes Soares C (2019) Uncertainty analysis of the hydrodynamic coefficients estimation of a non-linear manoeuvring model based on planar motion mechanism tests. Ocean Eng. 173, 450-459. https://doi.org/10.1016/j.oceaneng.2018.12.075

Xu H, Hassani V, Guedes Soares C (2020) Truncated least square support vector machine for parameter estimation of a non-linear manoeuvring model based on PMM tests. Appl. Ocean Res. 97, 102076. https://doi.org/10.1016/j.apor.2020.102076

Xu H, Hinostroza MA, Guedes Soares C (2021) Modified vector field path-following control system for an underactuated autonomous surface ship model in the presence of static obstacles. J. Mar. Sci. Eng. 9(6). https://doi.org/10.3390/jmse9060652

Xu H, Pires da Silva P, Guedes Soares C (2024) Effect of sampling rate in sea trial tests on the estimation of hydrodynamic parameters for a non-linear ship manoeuvring model. J. Mar. Sci. Eng., 12(3): 407. https://doi.org/10.3390/jmse12030407

Yang H, Deng F, He Y, Jiao D, Han Z (2020) Robust non-linear model predictive control for reference tracking of dynamic positioning ships based on non-linear disturbance observer, Ocean Eng, 215,107885. https://doi.org/10.1016/j.oceaneng.2020.107885

Yu J, Yao C, Liu L, Zhang Z, Feng D (2021) Assessment of full-scale KCS free running simulation with body-force models. Ocean Eng. 237, 109570

Zhang H, Zhang X, Bu R (2022) Sliding mode adaptive control for ship path following with sideslip angle observer. Ocean Eng. 251, 111106. https://doi.org/10.1016/j.oceaneng.2022.111106

Zhang X, Xiong W, Xiang X, Wang Z (2019) Real-time simulation of a rescue ship maneuvering in short-crested irregular waves. IEEE Access. 7, 133936-133950. https://doi.org/10.1109/ACCESS.2019.2941591

Zhang Z, Zhao Y, Zhao G, Wang H, Zhao Y (2021) Path-following control method for surface ships based on a new guidance algorithm. J. Mar. Sci. Eng. 9, 166. https://doi.org/10.3390/jmse9020166

Zhou Y, Daamen W, Vellinga T, Hoogendoorn SP (2020) Impacts of wind and current on ship behavior in ports and waterways: A quantitative analysis based on AIS data. Ocean Eng. 213, 107774. https://doi.org/10.1016/j.oceaneng.2020.107774

Zhu M, Hahn A, Wen YQ (2018) Identification-based controller design using cloud model for course-keeping of ships in waves. Engineering Applications of Artificial Intelligence. 75: 22-35. https://doi.org/10.1016/j.engappai.2018.07.011

Zhu M, Sun W, Hahn A, Wen Y, Xiao C, Tao W (2020) Adaptive modeling of maritime autonomous surface ships with uncertainty using a weighted LS-SVR robust to outliers. Ocean Eng. 200, 107053. https://doi.org/10.1016/j.oceaneng.2020.107053